

# Short Papers

## HaptiYarn: Development of an Actuator Yarn That Can Transform Everyday Textiles Into Haptic Devices

Pasindu Lugoda<sup>1</sup>, Richard Arm<sup>2</sup>, Angus Wooler, Lincoln Barnes, Ahmed Tamkin Butt<sup>3</sup>, Carlos Oliveira<sup>4</sup>, Arash Shahidi<sup>5</sup>, and William Navaraj<sup>6</sup>

**Abstract**—A method of providing localised haptic feedback at precise locations on the body, utilising a lightweight textile garment is presented in this short paper. The textile comprises of subtly integrated actuator yarns (HaptiYarns) which are controlled by electropneumatic circuitry. Each yarn has two functional layers, an inner porous textile layer with limited extensibility and a second, durable outer layer made from an extensible elastomer. The HaptiYarns can provide radial forces and a maximum radial displacement of  $28.09 \pm 0.14$  mm. It was found that the intrinsic addition of graphite powder (5% by weight), during elastomer preparation, offered better resistance to layer delamination and increased the ability of the yarn to withstand higher internal air pressures by 48%. Both the graphite-filled composite and the graphite free yarns demonstrated high durability, withstanding cyclic testing of >7500 cycles while having no significant impact on the force feedback. Finally, a wearable prototype knitted textile garment is presented with eight HaptiYarns subtly integrated within it and connected to a virtual reality (VR) program providing an immersive haptic experience. These yarns offer the potential to transform everyday clothing into wearable haptic devices with potential to revolutionise healthcare, VR-based training, gaming, and entertainment sectors.

**Index Terms**—Haptics, elastomer, smart textiles, virtual reality, graphite-composite, tactile, metaverse.

### I. INTRODUCTION

THE demand for fully immersive experiences in virtual and augmented reality has expedited the development of haptic devices [1], [2]. Haptic technologies have the potential to revolutionise human activities, training, and performance, addressing the needs of a range of applications that are significant for several industries. Potential applications include therapy, rehabilitation, robotic teleoperation, gaming/entertainment, enterprise and sports training [1], [2], [3], [4], [5]. More specifically, in therapeutic and rehabilitative applications, haptic devices may be utilised to assist individuals with sensory impairments such as deaf blindness, where tactile surfaces like brail are often relied upon for communication [6], [7]. Tactile sensing and haptic feedback

devices are useful for prosthetic training, intuitive control and for providing sensory force feedback in prostheses [8], [9].

Haptics encompasses everything related to the sense of touch [4]. The sense of touch allows humans to perform a myriad of tasks such as grasping, manipulating and by extension, differentiating between materials surfaces and characteristics as well as determining fragility or danger [4]. The sense of touch can be broadly characterised into kinaesthetic and cutaneous/tactile subsenses [4]. This work focuses on a haptic device that provides cutaneous tactile feedback. Human skin relies on tactile sensing to feel mechanical properties such as shape, pressure, surface texture, temperature, viscosity, shear and normal forces [4]. Numerous wearables have been created for providing tactile feedback [1], [9], [10], [11], [12], [13], [14], [15], [16]. Some of the representative devices are highlighted in Table I. Among these wearables, vibrotactile devices are the most widespread, utilising changes in frequency, amplitude, waveform or duration to deliver information [6], [7], [8], [17]. Off-the-shelf miniature motors [7], [8], variants of custom electromagnetic coil-based actuators [1], [6], [9], or multi-layer piezoelectric stacks [14] are typically used for vibrotactile haptic feedback. Haptic devices and arrays that capitalise on these technologies, especially when they are rigid, can feel bulky and heavy and can impede with the user's natural dexterity [1], [16]. Table I highlights various efforts by investigators to achieve high performance, conformability and light-weight.

In other, more elegant designs, electrostimulation has also been utilised to generate the sensation of touch using small electrical currents [1]. In these devices, it is often difficult to predict the appropriate current values since skin impedance fluctuates (sweat and hydration changes) and this can result in uncomfortable sensations and in some cases cause electrically induced lesions [16], [18]. Thermal cues have also been utilised to provide sensory feedback [5], but their applications are limited due to the nature of thermal dynamics in materials; where temperature changes respond slowly to input variations which delays the response time of the wearable device [5].

Another way to provide tactile feedback is using static indentation. The detection threshold for static indentation can vary based on the user, the area of indentation and the interacting object [13]. Average threshold for detection of static indentation in human skin is  $\sim 50$ – $100$   $\mu\text{m}$  [13]. A majority of the conformable wearable haptic actuators in the literature aims to exceed this threshold [13], [16]. Most of these devices achieve a maximum displacement of a few millimetres [19], whereas human skin is capable of far higher deformations. The human gluteal tissue, for example, can comfortably deform up to 44 mm without causing discomfort [20]. This raises additional questions about the effectiveness of full body haptic feedback applications for the future. Apart from sub-millimetre indenting high resolution static and dynamic haptic actuators, there is a need for conformal haptic

Manuscript received 4 September 2023; revised 6 December 2023; accepted 26 February 2024. Date of publication 4 March 2024; date of current version 19 December 2024. This paper was recommended for publication by Associate Editor K. Kyung and Editor-in-Chief S. Choi upon evaluation of the reviewers' comments. (Corresponding author: Pasindu Lugoda.)

Pasindu Lugoda, Angus Wooler, Lincoln Barnes, Ahmed Tamkin Butt, and William Navaraj are with the Department of Engineering, School of Science and Technology, Nottingham Trent University, NG11 8NF Nottingham, U.K. (e-mail: pasindu.lugoda@ntu.ac.uk; angus.wooler2019@my.ntu.ac.uk; lincoln.barnes2019@my.ntu.ac.uk; ahmed.butt@ntu.ac.uk; william.navaraj@ntu.ac.uk).

Richard Arm, Carlos Oliveira, and Arash Shahidi are with the Advanced Textiles Research Group, Flexural Composites Research Laboratory, School of Art and Design, Nottingham Trent University, NG1 4GG Nottingham, U.K. (e-mail: richard.arm@ntu.ac.uk; jose.oliveira@ntu.ac.uk; arash.shahidi@ntu.ac.uk).

This article has supplementary downloadable material available at <https://doi.org/10.1109/TOH.2024.3371831>, provided by the authors.

Digital Object Identifier 10.1109/TOH.2024.3371831

TABLE I  
COMPARISON OF VARIOUS REPRESENTATIVE WEARABLE HAPTIC TECHNOLOGIES

Ref.	Demonstrated Application(s)	Actuator Density	Weight	Actuation Modality	Key figure of merits	Key comparison with this work
[12]	-	3 actuators for the fingertip	~30 g	3 motors for achieving 3DoF cutaneous force feedback	1.5 N	Rigid components, not shearable
[1]	Virtual/augmented reality	~0.3-0.4 cm <sup>-2</sup>	~4 g/actuator in a 32-element array	Electromagnetic coil-based actuation for vibrotactile cutaneous feedback	Dynamic displacement amplitude ~15 μm	Only vibrotactile feedback, not shearable
[9]	GPS-based haptic navigation system, auditory/music interface, prosthetic haptic feedback	0.73 cm <sup>-2</sup>	~0.8 g/actuator in a 127-element array	Electromagnetic coil-based eccentric rotating mass (ERM) motors for vibrotactile cutaneous feedback	Maximum vertical displacement of 0.35mm	Only vibrotactile feedback only, rigid components
[14]	Wireless telehaptics	~5.6 cm <sup>-1</sup>		Submillimeter multi-stack piezoelectric (PZT) actuator for cutaneous feedback	1 Hz to 1 kHz, <1.55 ms actuation time	Only vibrotactile feedback, not shearable
[15]	-	20 mm dia.	~60 g for 3x5 array	Dielectric elastomer actuator array embedded in textile	Thickness 7 mm	Only vibrotactile feedback
[13]	-	~2 cm <sup>-1</sup> (5 mm dia.)	Max 1 g/actuator	3D printed Stretchable Hydraulically amplified electrostatic actuators	Static Radial Displacement ~200 μm Force ~30 mN	Radial displacement ~200 μm
[16]	Surface texture/object shape recognition	~3.3 cm <sup>-1</sup>		Stretchable pressure-amplified hydraulic electrostatic actuators for cutaneous feedback	Static Radial Displacement ~500 μm and Output pressure ~1 MPa.	Radial displacement ~500 μm
[19]	Haptics display sleeve and camouflage	4 mm pitch	~55g for 32 x 24 flexible array skin	SMP based actuator array	Max static displacement ~2mm 2.5 s switching time	radial displacement~2 mm, not shearable
[23]	Interactive morphing textiles (Eg. Onbody display, breath regulation)	Fibre diameter <1.8mm		OmniFiber: Contractible/extendable fluidic artificial fibre muscle (pneumatic)	Transverse force and displacement up to 19 N at 0.5 MPa, linear actuation speed 150mm/s (peak)	Transverse force and displacement, linear actuation
This work	Virtual/augmented reality	Fibre diameter 4.56 ± 0.07 mm	3.22 ± 0.09 g silicone yarn (18 cm) 3.59 ± 0.16 g - 5% graphite-filled silicone yarn (18 cm)	Pneumatic HaptiYarn	Radial force and static radial displacement (maximum-28.09±0.14 mm) Seamless integration within textiles	Key achievements: Shearable, high static radial displacement (maximum-28.09±0.14 mm)

actuators that can achieve high displacements (up to tens of millimetres) whilst maintaining comfort for the user. The principles and prototypes introduced in this paper will focus on both comfort and dynamic displacement. Companies such as Meta and HaptX have utilised miniature bladders to manufacture smart gloves. These devices use elastomers to deliver feedback. A discreet method of creating wearable haptics is to seamlessly integrate these devices within everyday clothing, creating smart textiles. Smart textiles' have garnered considerable interest in

recent years owing to their attributes of being flexible, lightweight, and portable [21]. Due to these reasons, smart textiles technologies have been developed for haptic applications [11], [17], [22], [23], [24], [25], [26], [27]. Some of these devices have non-ideal and rather bulky electronics and mechanical structures attached on the surface of the textile [27], [28]. This affects the conformability of the textiles, which has a direct impact on the wearer's comfort and can impede with the user's dexterity. More inconspicuous techniques that provide

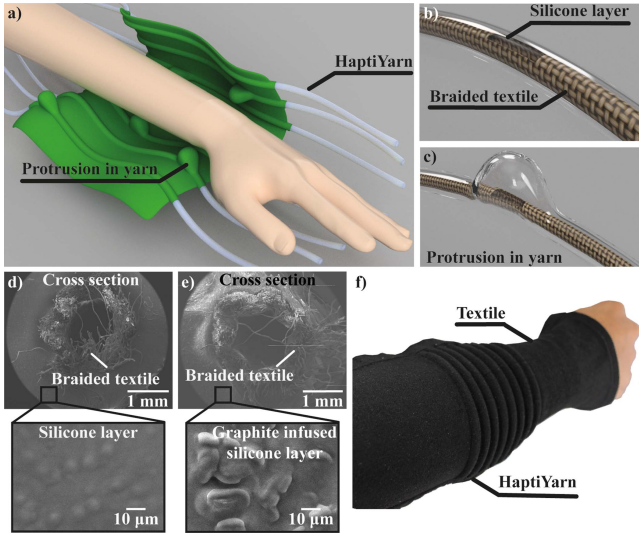


Fig. 1. Demonstration of the novel approach used to develop the wearable haptic textile concept. (a) A concept figure of the user interaction with haptic textile created using several HaptiYarns. (b) A schematic of the HaptiYarn deflated. (c) A schematic of the HaptiYarn inflated. (d) A cross-sectional view of HaptiYarn taken using a SEM. The magnified view of the silicone region without added graphite, showing a smoother surface micro-structure. (e) A cross-sectional SEM image of a graphite-filled HaptiYarn. The magnified view of the graphite-filled silicone region of the HaptiYarn showing a rougher surface micro-structure. (f) The working, proof-of-concept prototype created using eight HaptiYarns embedded within a comfortable, breathable knitted textile.

soft robotic actuation in textiles have been developed, [23], [25], [29] such as the McKibben actuator which utilises an elastic tube and a braided sleeve to compress and extend like a muscle [23]. Nonetheless, all these actuators can only make the textile perform mechanical deformations such as bending, straightening, contracting, and expanding. These devices do not provide localised radial mechanical force feedback (via indentation).

We present a comfortable and conformable smart textile approach for delivering localized force tactile feedback (with static radial displacements exceeding tens of millimeters) at specific body points. The smart textile was fabricated with tubular hollow yarns encapsulated within an elastomeric layer and positioned within a knitted elastodiene nylon fabric (schematically illustrated in Fig. 1(a)). The difference of these HaptiYarns in comparison to the prior art is illustrated in Table I. These HaptiYarns can be integrated within any garment such as armbands, t-shirts, or gloves. The yarns comprise of two functional layers. One of these layers is a porous textile layer with limited extensibility/stretchability and the second is a highly stretchable polymer layer. For this short paper, the porous textile layer was created by braiding polyester fibres. This creates a tubular textile structure which was then encapsulated with the stretchable material. Platinum-catalysed silicone was utilised as the stretchable material. As illustrated in the schematic Fig. 1(b), a part of the textile layer was removed using a laser cutter prior to the encapsulation. However, it is important to note that the wall thickness of the yarn remains the same despite the absence of the textile tube. This is because silicone flows within the pores and gaps in the textile layer creating a uniform thickness. The area that does not contain the textile layer expands when air pressure is applied from within the yarn, and this is demonstrated in the schematic Fig. 1(c). A scanning electron microscope (SEM) image of the cross section of the yarn is shown in Fig. 1(d). This illustrates the silicone outer layer surrounding the textile layer. The magnified microscopic image of the silicone layer

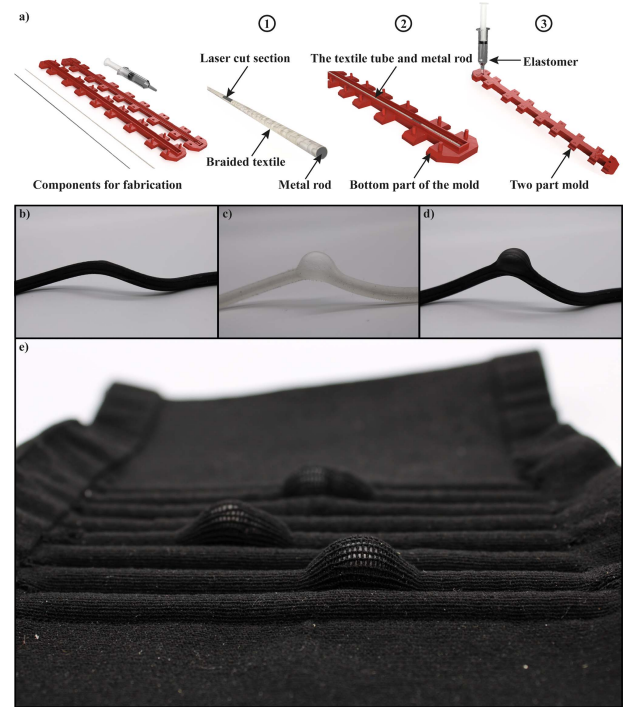


Fig. 2. Fabrication process of the HaptiYarns: (a) Initially, the textile tube is placed over a removable metal rod (mandrel). A laser is used to cut a hole in the textile tube. Thereafter the metal rod with the textile tube is positioned within a two-part mould. The silicone mixture is prepared, degassed, and injected into the mould. Once the elastomeric layer is fully cured, the finished HaptiYarn is removed from the mould and the steel mandrel is carefully withdrawn. (b) The deflated graphite powder filled silicone HaptiYarn. (c) A typical inflated silicone HaptiYarn. (d) A typical inflated graphite powder filled silicone HaptiYarn. (e) The knitted textile created using eight HaptiYarns embedded within the structure. The image shows typical inflations of three yarns.

shows the smoothness of the material. Graphite-composited silicone was also trialled as the stretchable material. This was done to identify the impact of increasing the tensile strength of the elastomer on the actuator performance. Graphite powder and graphite derivatives have been found to enhance the mechanical properties such as tensile strength in silicones [30]. The cross-section of a graphite-filled silicone HaptiYarn is given in Fig. 1(e). The magnified microscopic image of the graphite-filled silicone illustrates that the material is significantly rougher in comparison to the silicone. A demonstrator was created using eight of these HaptiYarns (Fig. 1(f)). These yarns were inserted within the knitted tubes of a textile. A video of the functional prototype interfaced to a rainfall virtual reality (VR) environment is shown in supplementary video 1 available online. The user interacting with the VR environment could feel the rain thanks to the HaptiYarns.

## II. METHODS

The fabrication technique of the HaptiYarn is schematically illustrated in Fig. 2(a). A final HaptiYarn is given in Fig. 2(b). The stretchable silicone layer of the HaptiYarn was created using a commercially available platinum-based silicone gel. Fig. 2(c) and (d) display an inflated silicone HaptiYarn and a graphite powder filled silicone HaptiYarn respectively. Silicone with a 0030 Shore hardness (Ecoflex 0030, Smooth-on, PA, USA) was chosen as the elastomer due to its softness, high extensibility, biocompatibility, and low viscosity.

The HaptiYarn was fabricated by placing a braided textile tube over a solid steel rod of diameter  $1.524 \pm 0.005$  mm. The braided textile

tube was created using a suture braider (lay length = 7; RU1/24-80, Herzog GmbH, Oldenburg, Germany). The covering braided structure consisted of 24 carriers with polyester yarns ( $2 \times 36$  filaments/167 dtex; Ashworth and Sons, Cheshire, U.K.). Thereafter a rectangular section (slit) of the braid having a length of  $10.23 \pm 0.39$  mm and width of 0.8 mm was cut off using a laser cutter. This size was chosen to prove the HaptiYarn concept. Then the whole structure was positioned in a prefabricated mould and filled with liquid silicone elastomer. To prevent air bubble formation a vacuum chamber was used during the fabrication after material mixing and prior to injection into the moulds. Once the silicone had cured, the elastomeric HaptiYarn was demoulded. Then the steel rod mandrel was removed from the structure creating the hollow HaptiYarn. The fabrication process is shown in the supplementary video 4 available online.

#### A. Fabrication of the Graphite-Filled Silicone HaptiYarns

Graphite powder was added to the silicone during liquid phase of preparation. Four different percentages of graphite powder were tested, and they were 1%, 2%, 3% and 5%. These percentages were calculated by weight. Initially the graphite powder ( $<20 \mu\text{m}$ , Sigma-Aldrich, St. Louis, Missouri, United States) was mixed with part A of silicone and stirred for 1h using a magnetic stirrer. Then part B was added and stirred for another 10 mins. This mixture was then poured into the prefabricated mould by using the same procedure as previously described for the silicone HaptiYarns.

#### B. Experiments to Measure the Performance of HaptiYarns

To determine functional limits of the HaptiYarns, it was crucial to identify the maximum internal air pressure and the maximum radial expansion the yarns can withstand. To study this, yarns were inflated to their bursting points and the internal pressure within the yarn was measured. The radial displacements of the yarns were also measured using a CCD camera (60 frames per second,  $4000 \times 3000$  pixels resolution) and a visual guide (ruler 1mm resolution). A custom-built test rig was created for these experiments. The test rig utilized a 30 ml syringe to provide the air for the HaptiYarn. A linear actuator was used to control the amount of air injected into the tubes. The internal pressure within the HaptiYarn was measured using a pressure sensor (MPX2200AP, Freescale Semiconductor, Austin, Texas, USA). The external pressure generated by the HaptiYarn was captured using a load cell (FC2231-0000-0010-L, TE Connectivity, Schaffhausen, Switzerland). The measurements from the load cell and pressure sensor were measured using two DMM6500 6.5-digit Digital Multimeters (Keithley Instruments, Cleveland, Ohio, USA). Programs in LabVIEW (National Instruments, Austin, Texas, USA) and Arduino (Arduino, Turin, Italy) were created to control the linear actuator and capture the data from the multimeters. Three different samples were tested for silicone yarns and two to three different samples were tested for each percentage of the graphite-filled samples (1%–5%).

#### C. Tensile Tests Conducted on Silicone and Graphite-Filled Silicone Membrane

To examine the mechanical influence of graphite loading on the silicone membranes, agreed test standards were adapted. In uniaxial tests, all specimens were cut into dumbbell-shaped pieces using an ISO37:2017-1 approved die stamp. Specimens were secured to the tensile testing machine using clamping ‘method A’ as stated in the standard (ASTM D412-16(2021)2 and BS ISO 5893:20023). The thickness for each specimen was recorded using a digital microscope (Keyence VHX5000) at  $\times 50$  magnification and was used to calculate the true stress strain values. The grip-to-grip separation of the clamping jaws

was 25 mm, the preload was set to 0.05 N to remove slack from the specimens before data gathering began and the test speed was 50 mm/min. Specimen test temperature was ambient  $22 \text{ }^\circ\text{C}$  and humidity was 66%. All uniaxial specimens in each group were tested to failure in extension. The specimen preparation and test methods, loads and speeds were chosen as per the standard, but also to align results with other studies conducted with the same equipment and test parameters [31]. A Zwick Roell Z2.5 (Ulm, Germany) tensile testing machine was utilised for the testing. The tensile tests were conducted on three silicone and 5% graphite-filled silicone dumbbell-shaped samples.

#### D. Tensile Tests for Quantifying the Adhesion/Friction Between the Elastomer Membrane and the Textile

For the adhesion tests the authors were not aware of any specific test standards that can relate to this work. Therefore, new test protocols were set up for this experiment. Here, specialised sample tubes were created where approximately half of the tube only contained the elastomer (silicone or 5% graphite-filled silicone) and the second half comprised of the textile braided tube encapsulated with the elastomer. This was conducted by positioning the braided textile halfway up the metal rod (100 mm). It ensured that half of the tube was fabricated using only the elastomer. At the end with the braided textile, a portion of the textile tube was left unencapsulated. Thereafter, the elastomer only section and the unencapsulated textile braid were positioned within the grips of the tester. For the experiment the textile braided tube was pulled out of the elastomeric layer and the forces required for the delamination to occur was recorded. The adhesion tests were conducted on an AG-XD plus Shimadzu tensile testing machine (Kyoto, Japan). The tensile tester was operated at a test speed of 100 mm/min, and a preload of 0.5 N was used to remove slack from the specimens. The grip-to-grip separation of the clamping jaws was set at 150 mm. Five different samples were tested for the silicone samples and the once filled with 5% graphite powder.

#### E. Creating the VR Haptic Demonstrator

The demonstrator was created using eight HaptiYarns. These yarns were inserted within a prefabricated textile fabric. The fabric was knitted using a Stoll ADF 3 E7.2-gauge machine (Stoll, Baden-Württemberg, Germany) using elastodiene nylon yarns (58% nylon 42% elastic core, nylon 78 /  $18 \times 1$ , elastic core 90, Yeoman yarns, Leicester, U.K.). The fabric had a single Jersey structure with integrated tubular channels for insertion of HaptiYarns. A 1 mm gap was present in between each channel. Regarding the interface electropneumatic circuit, each of the HaptiYarns were connected to a 3-way micro solenoid air valve (Fa0520E, DC- 6.0 V). The solenoid valves were connected to a mini air pump (ZR370-02PM, DC-4.5V) using tubes. The solenoid valves and the air pump were controlled using an Arduino MKR WiFi 1010. A program was coded in Arduino to control each of the tubes. The VR environment to interact with the textile was created in Unity (Unity Technologies, San Francisco, California, USA) using the programming language C#.

### III. RESULTS

The change in radial displacement with regards to input air volume for one representative sample for each percentage of graphite is illustrated in Fig. 3(a). The graph demonstrates that the expansion increases gradually with increasing air volume, then it is followed by a steep rise prior to approaching a plateau and the actuator bursting. The average displacement recorded for the silicone, 1%, 2%, 3% and 5% samples were  $15.5 \pm 0.47$ mm,  $4.23 \pm 1.34$  mm,  $18.00 \pm 1.07$  mm,

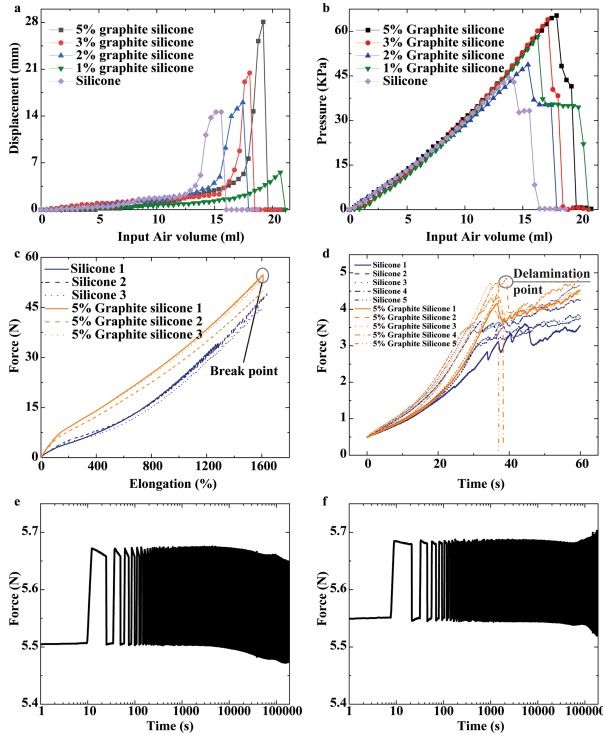


Fig. 3. Experimental results from HaptiYarns. (a) The indentation measurements from the bursting test for HaptiYarns with varying percentages of added graphite powder. (b) Change in internal pressure during the bursting test recorded for the different percentages of graphite powder. (c) The tensile test results from silicone and graphite-filled silicone dumbbell-shaped samples. (d) Tensile test characteristics of the silicone samples, and the 5% graphite-filled silicone samples to identify the delamination points. (e) The performance of the silicone HaptiYarn when subjected to a cyclic test (more than 7500 cycles). (f) Cyclic test results from the 5% graphite powder filled silicone HaptiYarn (more than 7500 cycles).

$20.54 \pm 1.25$  mm, and  $25.12 \pm 2.96$  mm respectively. The 5% graphite-filled samples demonstrated the highest indentation, and one 5% sample exhibited a maximum displacement of 28.09 mm.

The average internal bursting (peak) pressure recorded for the silicone HaptiYarns were  $47.0 \pm 2.6$  kPa, while the average internal bursting pressure for the graphite powder filled yarns were  $55.4 \pm 4.6$  kPa,  $54.4 \pm 5.4$  kPa,  $61.5 \pm 2.25$  kPa,  $67.0 \pm 1.4$  kPa for the 1%, 2%, 3% and 5% samples respectively. Data from a single representative sample for each percentage of added graphite powder is shown in Fig. 3(b). It was observed from the results that filling the silicone structure with graphite powder strengthened the yarns and increased its ability to withstand higher internal pressures (48% higher for 5% graphite-filled yarns). The internal bursting pressure for the yarns was higher with graphite-filled samples compared to silicone ones. It was observed that the purely silicone samples resulted in a higher displacement than the 1% graphite-filled sample but demonstrated a lower peak pressure than the 1% sample. Overall, addition of graphite results in increased strength of the elastomeric component of the yarn. This was further validated by the tensile test results illustrated in Fig. 3(c). These results also concur with the literature [30], and illustrates that 5% of graphite powder addition increased the amount of tensile strength of the silicone by 22.4%.

Another observation that was made during the burst test was that at high internal pressures the outer silicone layer delaminated from the inner polyester braided tubes. When the silicone actuator is constrained to expand through the smaller opening the pressure results in radial forces acting perpendicular to the yarn (causing the indentation)

as well as axial forces parallel to the yarn. If the axial forces can overcome the interfacial force between the yarn and the silicone, the silicone delaminates. The delamination results in more room for the silicone to expand (shown in supplementary video 2 available online). Delamination was significantly lower for the graphite filled samples that had a higher concentration of graphite powder (5% graphite-filled HaptiYarn shown in Supplementary video 3 available online). This can be attributed to tribological reasons, primarily due to increased surface roughness (Fig. 1(d)–(e)), resulting in an increase in the adhesion/friction between the textile layer and the outer silicone layer. To further understand the effect of graphite powder on the adhesion or friction an experiment was conducted. The results displayed in Fig. 3(d) illustrates that larger forces were required for the graphite-filled silicone samples to delaminate in comparison to the silicone samples without added graphite. The average forces required for the initial delamination was measured as  $3.27 \pm 0.31$  N and  $4.55 \pm 0.27$  N for the silicone samples and the 5% graphite-filled silicone samples respectively. This experiment concurs with our hypothesis that graphite fillers increased the adhesive or frictional bond between the elastomer and the textile fibre, which could be attributed mainly to the surface roughness causing an increased Van der Waals force. Further study is required to investigate whether any other chemical bonding force is involved beyond Van der Waals static friction.

When these yarns are used to create wearable haptic garments, each yarn must be able to effectively provide haptic feedback over a prolonged period. Hence, they must be able to withstand several cycles of providing tactile feedback and returning to their relaxed state. To test product durability, yarns were subjected to cyclic tests of more than 7500 cycles. The internal pressure was cycled from atmospheric pressure to  $30.8 \pm 0.5$  kPa above atmospheric pressure. The results from the cyclic tests are shown in Fig. 3(e) and (f). It can be observed that both the silicone yarns and 5% graphite-filled silicone yarns were robust and able to withstand a prolonged cyclic test. The external pressure created by the indentation in the silicone yarn during the first cycle was measured at 0.167 N and the external force created at the 7550 cycle was recorded as 0.172 N. Similarly, the force exerted by the protrusion in the 5% graphite-filled silicone yarn was measured at 0.136 N at the start of the cyclic test and at the end of 7550 cycles it produced a force of 0.157 N. This illustrates that there is no degradation in the force applied by the two HaptiYarns even after 7500 cycles of expansion.

Future work must investigate the impact of using graphite concentration greater than 5%, along with exploring the influence of using different elastomers (such as thermoplastic polyurethane or other silicones with different mechanical properties). It is envisaged that different slit sizes (laser cut sections) must be explored to identify the impact of this on the performance of the yarns. Moreover, larger sample sizes must be created and better particle distribution methods (such as using a centrifugal mixture) should be explored to ensure better homogeneity in the graphite-filled membranes. The impact on delamination when the braided textile layer is created using textile fibres (like cotton) with higher surface roughness's must be investigated. Moreover, knitting and weaving techniques need to be explored to identify methods of creating 2D textile-based haptic arrays using these yarns.

The proof-of-concept demonstrator for the realized HaptiYarn array has the centres of two consecutive yarns positioned  $9.28 \pm 0.17$  mm apart. Hence, this array is better suited for providing haptic feedback in non-glabrous areas of human skin, where mechanoreceptors are sparse, as indicated by the 2-point discrimination threshold exceeding a centimeter for most regions [32], [33]. Future research should investigate techniques for reducing the distance between yarns by minimising the yarn dimensions. Furthermore, for this study as a proof of concept the HaptiYarn array was interfaced with a VR environment. In the future it is crucial to investigate the usability of these yarns when simulating

tactile interactions in various VR environments. To achieve this, further extensive user trials must be conducted with repeated texture and object classification tasks. Through these trials, optimal slit patterns, material combinations and fabric construction techniques can be established for delivering these tactile interactions.

#### IV. CONCLUSION

We have presented a haptic actuator textile achieved by integrating a haptic yarn within it. A maximum radial displacement of  $28.09 \pm 0.14$  mm was achieved utilising these yarns. The yarns were created using two functional layers. One of these layers is a porous textile layer with limited extensibility and the second is a highly stretchable silicone layer. It was observed that filling the stretchable silicone layer with higher percentages of graphite powder increased the peak radial displacement through the slit opening of the HaptiYarn. This can be attributable to both the increase in delamination resistance and increase in the strength of the silicone layer due to the added graphite powder [30]. The HaptiYarns with and without graphite powder saturation were able to withstand more than 7500 cycles. The feedback force provided by HaptiYarns was not impacted by the cyclic tests. Therefore, these HaptiYarns can interface with VR and create more immersive environments for numerous applications.

#### ACKNOWLEDGMENT

The authors want to thank Damien Goy and Jack Stapleton-Varga for their assistance with tensile testing and mould design. Support from Nottingham Trent University is acknowledged.

#### REFERENCES

- [1] X. Yu et al., "Skin-integrated wireless haptic interfaces for virtual and augmented reality," *Nature*, vol. 575, no. 7783, pp. 473–479, 2019, doi: [10.1038/s41586-019-1687-0](https://doi.org/10.1038/s41586-019-1687-0).
- [2] T. Yang, J. R. Kim, H. Jin, H. Gil, J. Koo, and H. J. Kim, "Recent advances and opportunities of active materials for haptic technologies in virtual and augmented reality," *Adv. Funct. Mater.*, vol. 31, no. 39, 2021, Art. no. 2008831, doi: [10.1002/adfm.202008831](https://doi.org/10.1002/adfm.202008831).
- [3] M. Aggravi, C. Pacchierotti, and P. R. Giordano, "Connectivity-maintenance teleoperation of a UAV fleet with wearable haptic feedback," *IEEE Trans. Automat. Sci. Eng.*, vol. 18, no. 3, pp. 1243–1262, Jul. 2021, doi: [10.1109/TASE.2020.3000060](https://doi.org/10.1109/TASE.2020.3000060).
- [4] T. A. Kern, C. Hatzfeld, and A. Abbasimoshaei, Eds., *Engineering Haptic Devices*. Berlin, Germany: Springer, 2023, doi: [10.1007/978-3-031-04536-3](https://doi.org/10.1007/978-3-031-04536-3).
- [5] J. Oh, S. Kim, S. Lee, S. Jeong, S. H. Ko, and J. Bae, "A liquid metal based multimodal sensor and haptic feedback device for thermal and tactile sensation generation in virtual reality," *Adv. Funct. Mater.*, vol. 31, no. 39, 2020, Art. no. 2007772, doi: [10.1002/adfm.202007772](https://doi.org/10.1002/adfm.202007772).
- [6] O. Ozioko, W. Navaraj, M. Hersh, and R. Dahiya, "Tacsac: A wearable haptic device with capacitive touch-sensing capability for tactile display," *Sensors*, vol. 20, no. 17, Aug. 2020, Art. no. 4780, doi: [10.3390/s20174780](https://doi.org/10.3390/s20174780).
- [7] O. Ozioko, W. T. Navaraj, M. Hersh, and R. Dahiya, "SmartFinger-Braille: A tactile sensing and actuation based communication glove for deafblind people," in *Proc. IEEE 26th Int. Symp. Ind. Electron.*, 2017, pp. 2014–2018.
- [8] W. T. Navaraj, O. Ozioko, H. Nassar, and R. Dahiya, "Prosthetic hand with biomimetic tactile sensing and force feedback," in *Proc. IEEE-Int. Symp. Circuits Syst.*, 2019, pp. 1–4.
- [9] Y. H. Jung et al., "A wireless haptic interface for programmable patterns of touch across large areas of the skin," *Nature Electron.*, vol. 5, no. 6, pp. 374–385, May 2022, doi: [10.1038/s41928-022-00765-3](https://doi.org/10.1038/s41928-022-00765-3).
- [10] P. B. Shull and D. D. Damian, "Haptic wearables as sensory replacement, sensory augmentation and trainer—A review," *J. Neuroengineering Rehabil.*, vol. 12, no. 1, pp. 1–13, Jul. 2015, doi: [10.1186/S12984-015-0055-Z/FIGURES/7](https://doi.org/10.1186/S12984-015-0055-Z/FIGURES/7).
- [11] N. K. Persson, J. G. Martinez, Y. Zhong, A. Maziz, and E. W. H. Jager, "Actuating textiles: Next generation of smart textiles," *Adv. Mater. Technol.*, vol. 3, no. 10, Oct. 2018, Art. no. 1700397, doi: [10.1002/ADMT.201700397](https://doi.org/10.1002/ADMT.201700397).
- [12] D. Prattichizzo, F. Chinello, C. Pacchierotti, and M. Malvezzi, "Towards wearability in fingertip haptics: A 3-DoF wearable device for cutaneous force feedback," *IEEE Trans. Haptics*, vol. 6, no. 4, pp. 506–516, Oct.–Dec. 2013, doi: [10.1109/TOH.2013.53](https://doi.org/10.1109/TOH.2013.53).
- [13] G. Grasso, S. Rosset, H. Shea, G. Grasso, H. Shea, and S. Rosset, "Fully 3D-printed, stretchable, and conformable haptic interfaces," *Adv. Funct. Mater.*, vol. 33, no. 20, May 2023, Art. no. 2213821, doi: [10.1002/ADFM.202213821](https://doi.org/10.1002/ADFM.202213821).
- [14] H. Jin et al., "Highly pixelated, untethered tactile interfaces for an ultraflexible on-skin telehaptic system," *NPJ Flexible Electron.*, vol. 6, no. 1, pp. 1–11, Sep. 2022, doi: [10.1038/s41528-022-00216-1](https://doi.org/10.1038/s41528-022-00216-1).
- [15] D. Y. Lee et al., "A wearable textile-embedded dielectric elastomer actuator haptic display," *Soft Robot.*, vol. 9, no. 6, pp. 1186–1197, Dec. 2022, doi: [10.1089/SORO.2021.0098](https://doi.org/10.1089/SORO.2021.0098).
- [16] S. Chen, Y. Chen, J. Yang, T. Han, and S. Yao, "Skin-integrated stretchable actuators toward skin-compatible haptic feedback and closed-loop human-machine interactions," *NPJ Flexible Electron.*, vol. 7, no. 1, pp. 1–12, Jan. 2023, doi: [10.1038/s41528-022-00235-y](https://doi.org/10.1038/s41528-022-00235-y).
- [17] Z. Li et al., "Air permeable vibrotactile actuators for wearable wireless haptics," *Adv. Funct. Mater.*, vol. 33, no. 8, 2023, Art. no. 2211146, doi: [10.1002/adfm.202211146](https://doi.org/10.1002/adfm.202211146).
- [18] S. F. Cogan, "Neural stimulation and recording electrodes," *Annu. Rev. Biomed. Eng.*, vol. 10, pp. 275–309, 2008, doi: [10.1146/annurev.bioeng.10.061807.160518](https://doi.org/10.1146/annurev.bioeng.10.061807.160518).
- [19] N. Besse et al., "Flexible active skin: Large reconfigurable arrays of individually addressed shape memory polymer actuators," *Adv. Mater. Technol.*, vol. 2, no. 10, Oct. 2017, Art. no. 1700102, doi: [10.1002/ADMT.201700102](https://doi.org/10.1002/ADMT.201700102).
- [20] C. Then et al., "A method for a mechanical characterisation of human gluteal tissue," *Technol. Health Care*, vol. 15, no. 6, pp. 385–398, 2007, doi: [10.3233/thc-2007-15601](https://doi.org/10.3233/thc-2007-15601).
- [21] A. Libanori, G. Chen, X. Zhao, Y. Zhou, and J. Chen, "Smart textiles for personalized healthcare," *Nature Electron.*, vol. 5, no. 3, pp. 142–156, Mar. 2022, doi: [10.1038/s41928-022-00723-z](https://doi.org/10.1038/s41928-022-00723-z).
- [22] V. Sanchez et al., "Textile technology for soft robotic and autonomous garments," *Adv. Funct. Mater.*, vol. 31, no. 6, Feb. 2021, Art. no. 2008278, doi: [10.1002/ADFM.202008278](https://doi.org/10.1002/ADFM.202008278).
- [23] O. K. Afsar et al., "OmniFiber: Integrated fluidic fiber actuators for weaving movement based interactions into the fabric of everyday life," in *Proc. 34th Annu. ACM Symp. User Interface Softw. Technol.*, 2021, pp. 1010–1026, doi: [10.1145/3472749.3474802](https://doi.org/10.1145/3472749.3474802).
- [24] S. Liu et al., "Textile electronics for VR/AR applications," *Adv. Funct. Mater.*, vol. 31, no. 39, Sep. 2021, Art. no. 2007254, doi: [10.1002/ADFM.202007254](https://doi.org/10.1002/ADFM.202007254).
- [25] L. Cappello et al., "Exploiting textile mechanical anisotropy for fabric-based pneumatic actuators," *Soft Robot.*, vol. 5, no. 5, pp. 662–674, Oct. 2018, doi: [10.1089/SORO.2017.0076](https://doi.org/10.1089/SORO.2017.0076).
- [26] H. Culbertson, S. B. Schorr, and A. M. Okamura, "Haptics: The present and future of artificial touch sensation," *Annu. Rev. Control, Robot., Auton. Syst.*, vol. 1, pp. 385–409, May 2018, doi: [10.1146/annurev-control-060117-105043](https://doi.org/10.1146/annurev-control-060117-105043).
- [27] M. Bianchi et al., "Design and preliminary affective characterization of a novel fabric-based tactile display," in *Proc. IEEE Haptics Symp.*, 2014, pp. 591–596, doi: [10.1109/HAPTICS.2014.6775522](https://doi.org/10.1109/HAPTICS.2014.6775522).
- [28] H. Culbertson, C. M. Nunez, A. Israr, F. Lau, F. Abnoui, and A. M. Okamura, "A social haptic device to create continuous lateral motion using sequential normal indentation," in *Proc. IEEE Haptics Symp.*, 2018, pp. 32–39, doi: [10.1109/HAPTICS.2018.8357149](https://doi.org/10.1109/HAPTICS.2018.8357149).
- [29] M. Zhu et al., "PneuSleeve: In-fabric multimodal actuation and sensing in a soft, compact, and expressive haptic sleeve," in *Proc. Conf. Hum. Factors Comput.*, 2020, pp. 1–12, doi: [10.1145/3313831.3376333](https://doi.org/10.1145/3313831.3376333).
- [30] J. Wang, X. Jin, C. Li, W. Wang, H. Wu, and S. Guo, "Graphene and graphene derivatives toughening polymers: Toward high toughness and strength," *Chem. Eng. J.*, vol. 370, pp. 831–854, Aug. 2019, doi: [10.1016/J.CEJ.2019.03.229](https://doi.org/10.1016/J.CEJ.2019.03.229).
- [31] R. Arm, A. Shahidi, and T. Dias, "Mechanical behaviour of silicone membranes saturated with short strand, loose polyester fibres for prosthetic and rehabilitative surrogate skin applications," *Materials*, vol. 12, no. 22, Nov. 2019, Art. no. 3647, doi: [10.3390/MA12223647](https://doi.org/10.3390/MA12223647).
- [32] F. Mancini et al., "Whole-body mapping of spatial acuity for pain and touch," *Ann. Neurol.*, vol. 75, no. 6, pp. 917–924, 2014, doi: [10.1002/ana.24179](https://doi.org/10.1002/ana.24179).
- [33] W. T. Navaraj et al., "Nanowire FET based neural element for robotic tactile sensing skin," *Front. Neurosci.*, vol. 11, 2017, Art. no. 501.